Journal Name

ARTICLE TYPE

Cite this: DOI: 00.0000/xxxxxxxxxx

Supplementary information

L. Klochko,*[a] V. Mandrolko,[b,a], G. Castanet[a], G. Pernot[a], F. Lemoine[a], K. Termentzidis[c], D. Lacroix[a] and M. Isaiev[a]

1 The model and simulation approaches

1.1 Molecular dynamics calculation

Simulation domain has size $30a_0 \times 10a_0 \times 42a_0$ in x,y, and z directions respectively, where $a_0 = 0.543$ nm is the lattice parameter for Si. Both systems consist of two silicon slabs with a slab of water. For the case of confined water (case i), the slab of water covers all silicon surface, and for the meniscus (case ii) it covers only the central part. All the systems consist of 67800 atoms of Si in total, but with variety of water molecules: 15028 for confined water, 3179 for meniscus with size $6a_0$, 5201 for meniscus with size $10a_0$, and 7225 for meniscus with size $14a_0$. The distance between two silicon slabs is set as $10a_0$.

Silicon was simulated as diamond lattice with lattice parameters of 0.543 nm and its surface is in contact with water with $(0,0,1)$ crystal plane. The interaction between silicon atoms were modeled via the Stillinger-Weber potential[1]. Atoms in the bottom and top of silicon slabs ($1.086 < z_1 < 2.172$ nm, $20.634 < z_2 < 21.72$ nm) were fixed with string forces to maintain their position close to the initial. The simple sketch that shows how input parameters are arranged compared to the system is showm in Fig. 1.

Water was simulated in frame of extended simple point charge model, SPC/E[2]. The interaction potential was determined by a combination of the Lennard-Jones, and the Coulombic potentials with cutoff distances $r_c = 1.0$ nm for both of them. For long-range Coulomb forces, each atom is assigned a charge such as $q(H) = +0.4238e$, and $q(O) = -0.8476e$. Usage of selected parameters give us a neutral charge for water molecules. To keep the O-H bond length, $l = 0.096$ nm, and H-O-H angles, 109.46°, sustainable the SHAKE algorithm was applied. For O-O interaction the values of $\varepsilon = 6.736$ meV, and σ = 0.3166 nm were chosen. In case of O-Si interaction, epsilon varied within 10 – 21 meV, and σ = 0.26305 nm.

Firstly, the initial system was tempered at temperature $T = 1$ K by using Gaussian distribution for velocity field. Then the system evolved in the NVE ensemble with a gradual temperature rescaling up to 300 K for 150 ps. (Temperature rescaling to 10 K was applied for 50 ps, to 50 K for 50 ps and finally to 300 K for another 50 ps). Further the systems were equilibrated in NVT ensemble for 150 ps.

After equilibration, temperature rescales to 270 K and 330 K were applied to the regions $2.172 < z < 3.801$ nm and $19.005 < z < 20.634$ nm respectively. Then the simulation was performed for 1 ns. The values of temperature, density, potential and kinetic energy of particles and stress tensors were obtained. The obtained values are averaged from all values calculated every 0.01 ps. The binning of the system was 0.2 nm. In the region with water, calculations were performed with binning 0.1 nm for more precise calculations of water density.

1.2 Usage of FEM procedure

In order to analyze the heat transfer, MD simulations were completed by a model based on the continuum heat diffusion equation.This model makes use of the finite element method (FEM) in COMSOL ® software to obtain the temperature field in the steady state inside the liquid meniscus and the Si slabs. The boundary conditions considered for the FEM simulations are summarised in Fig. 2. All the boundaries that confined the liquid meniscus and the SI slabs are thermally insulated, excepton at the top and bottom sides of the computational domain where uniform temperatures are imposed. The temperatures of the lower and upper boundaries were set at 330 K and 270 K respectively. A contact thermal resistance is also specified for the interfaces between the liquid and the solid, so that a discontinuity of temperature and heat flux is obtained at these interfaces. As an input, resistance values were taken from the results obtained from MD considering a specific value of ε. The thermal conductivity of silicon and water were chosen equal to 220 and 0.86 W/(m K) respectively to be consistent with with MD results. Special care was also taken for the geometry of the liquid meniscus, since the contact angle at the solid/liquid/gas triple junction must be consistent with the value of ε considered for the ITR. Finally, the position and the shape of the meniscus edges in the FEM simulations were adjusted to have a liquid volume that is equal to that considered in the MD simulations. An unstructured triangular mesh is used with elements size around 7.10^-2 nm. A convergence criterion = 0.001 (or relative tolerance on temperature) was applied to ensure a good accuracy of the results.

[a] *Université de Lorraine, CNRS, LEMTA, 54000 Nancy, France; E-mail: liudmyla.klochko@univ-lorraine.fr*

[b] *Faculty of Physics, Taras Shevchenko National University of Kyiv, 64/13, Volodymyrs'ka St., Kyiv 01601,Ukraine.*

[c] *Université de Lyon, CNRS, INSA-Lyon, CETHIL UMR5008, F-69621, Villeurbanne, France.*

† Electronic Supplementary Information (ESI) available: [details of any supplementary information available should be included here]. See DOI: 00.0000/00000000.

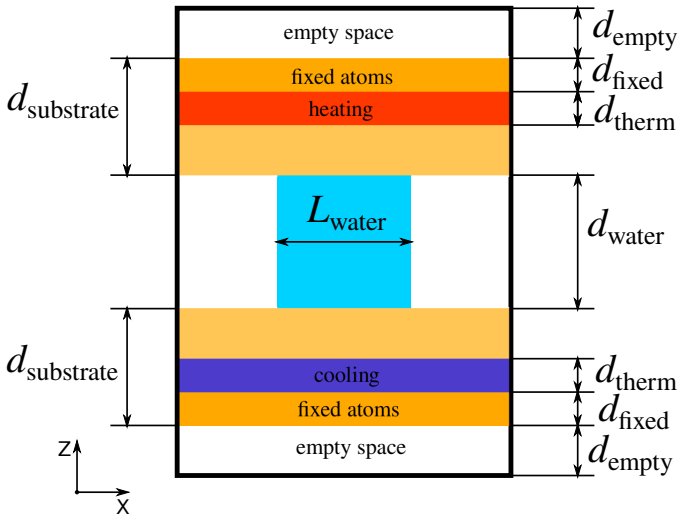

Fig. 1 Representation of the initial systems. Here L_{water} is the size of the initial systems cases i) $30a_0$, and ii) $6a_0$, $10a_0$,$14a_0$, $d_{\text{water}} = 10a_0$, $d_{\text{empty}} = 2a_0$, $d_{\text{fixed}} = 2a_0$, $d_{\text{substrate}} = 14a_0$, $d_{\text{therm}} = 3a_0$.

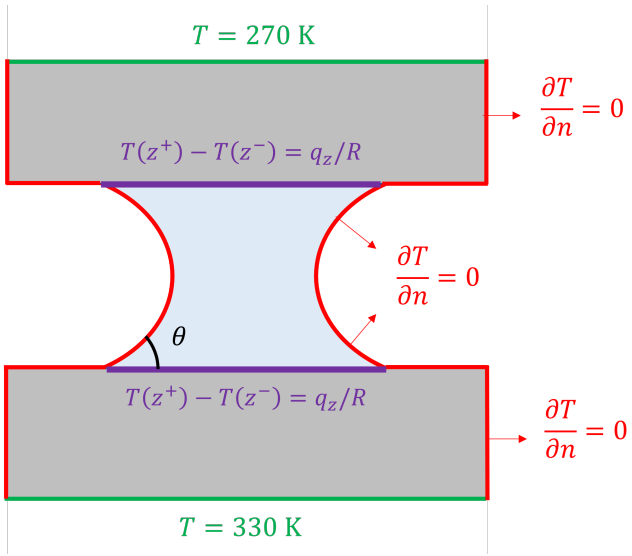

Fig. 2 Boundary conditions considered for the FEM modelling

2 A meniscus shape calculation

Curves corresponding to the boundaries of the droplets were obtained based on the circle approximation (see Fig. 3):

$$(x-x_0)^2 + (z-z_0)^2 = R^2_{\text{circle}},$$

where x_0 and z_0 – coordinates of the center of the circle. If d is the distance between silicon slabs, and ϕ is the wetting angle:

$$d/2 = R_{\text{circle}} \cos(\phi),$$

$$(x-x_0)^2 + (z-z_0)^2 = R^2_{\text{circle}},$$

$$(x-x_0)^2 + (z-z_0)^2 = d^2/(4\cos^2(\phi)),$$

$$x = x_0 \pm (d^2/(4cos^2(\phi) - (z-z_0)^2)^{1/2},$$

where the roots with "±" and sign corresponds to a hydrophobic (+) and hydrophilic (-) cases respectively. x_0 was calculated based on the fact that the volume v of the droplet for all cases remains constant.

We calculated the volume of the droplet based on the number of water molecules and its density.

$$\frac{v}{2b} = \int_0^{x_0 \pm (d^2/(4\cos^2(\phi)) - (z-z_0)^2)^{1/2}} \int_{-d/2}^{d/2} dxdz,$$

b is the thickness of droplet which is not used for curve fitting because we are considering a 2D system. After calculating the

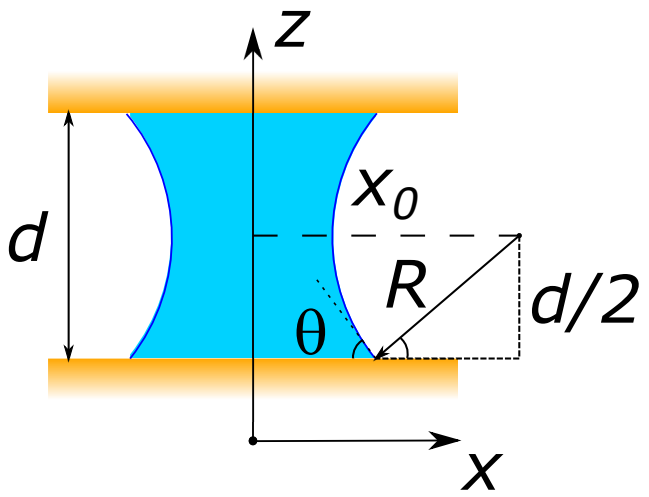

Fig. 3 A simple sketch that shows connection between curves corresponding to the boundaries of the droplets and the system, that we used to obtain curves in Figs.3, 11- 13. The input parameters that are shown here are well described in equation above.

integral, we obtain:

$$\frac{v}{2b} = x_0 d \pm \frac{1}{8}\Big[\frac{d^2}{\cos^2(\phi)} \cdot \arcsin\left(\frac{(2z_0+d)\cos(\phi)}{d}\right) - \\ - \frac{d^2}{\cos^2(\phi)} \cdot \arcsin\left(\frac{(2z_0-d)\cos(\phi)}{d}\right) + \\ + (d-2z_0)\sqrt{4z_0(d-z_0)+d^2\tan^2(\phi)} + \\ + (d+2z_0)\sqrt{-4z_0(d+z_0)+d^2\tan^2(\phi)}\Big]$$

Thus, we obtained an analytical equation of the curve bounding the drop based on the distance between the silicon slabs and the wetting angle.

3 Temperature profiles of the meniscus with heat fluxes distributions

The same temperature difference between two silicon slabs (60 K) was applied. Fig. 5 shows the temperature profiles with heat fluxes obtained using FEM (left) and MD (right) methods. The central plot shows one-dimensional temperature distributions in the middle of the system obtained from both of these approaches (solid green line represents FEM values and purple dots represents MD values). As it can be seen, the fluxes on the graph for MD are less structured than for FEM. This is expected due to fluctuations of physical quantities that are present in the MD simulation. Distribution for MD was obtained by averaging five simulations, each of them separately gives much more disordered fluxes. Averaging over more simulations would give the more directional fluxes with an increased computational costs.

The increase of the density peak near the surface with increasing ε is represented in Fig. **??** as well. Moreover, from Fig. **??**, it can be seen how water penetrates deeper into silicon for high ε. Increasing the ε creates a stronger coupling between water and silicon, which increases the depth of water penetration into the silicon lattice, and the density of the surface layer of water, which in turn reduces the mismatch in the density of vibration states and provides better heat transfer.

4 Effect of surface temperature on temperature jump

In order to make sure that the change in temperature jump, and hence thermal resistance with meniscus size, is not related to the different surface temperature depending on the meniscus size, the dependence of the surface temperature on ε was investigated. The results are presented in Fig. 4.

As can be seen from graphs (a) and (b), the surface temperature depends on the size of the meniscus. However, we considered the thermal jump as the average value between the hotter (T=330K) and colder (T=270K) sides. The averaged values (c) are within errors and the difference between the lowest and the highest value equal to 1 K which can't significantly affect the temperature jump. Therefore, the effect of the surface temperature change on the temperature jump is negligible.

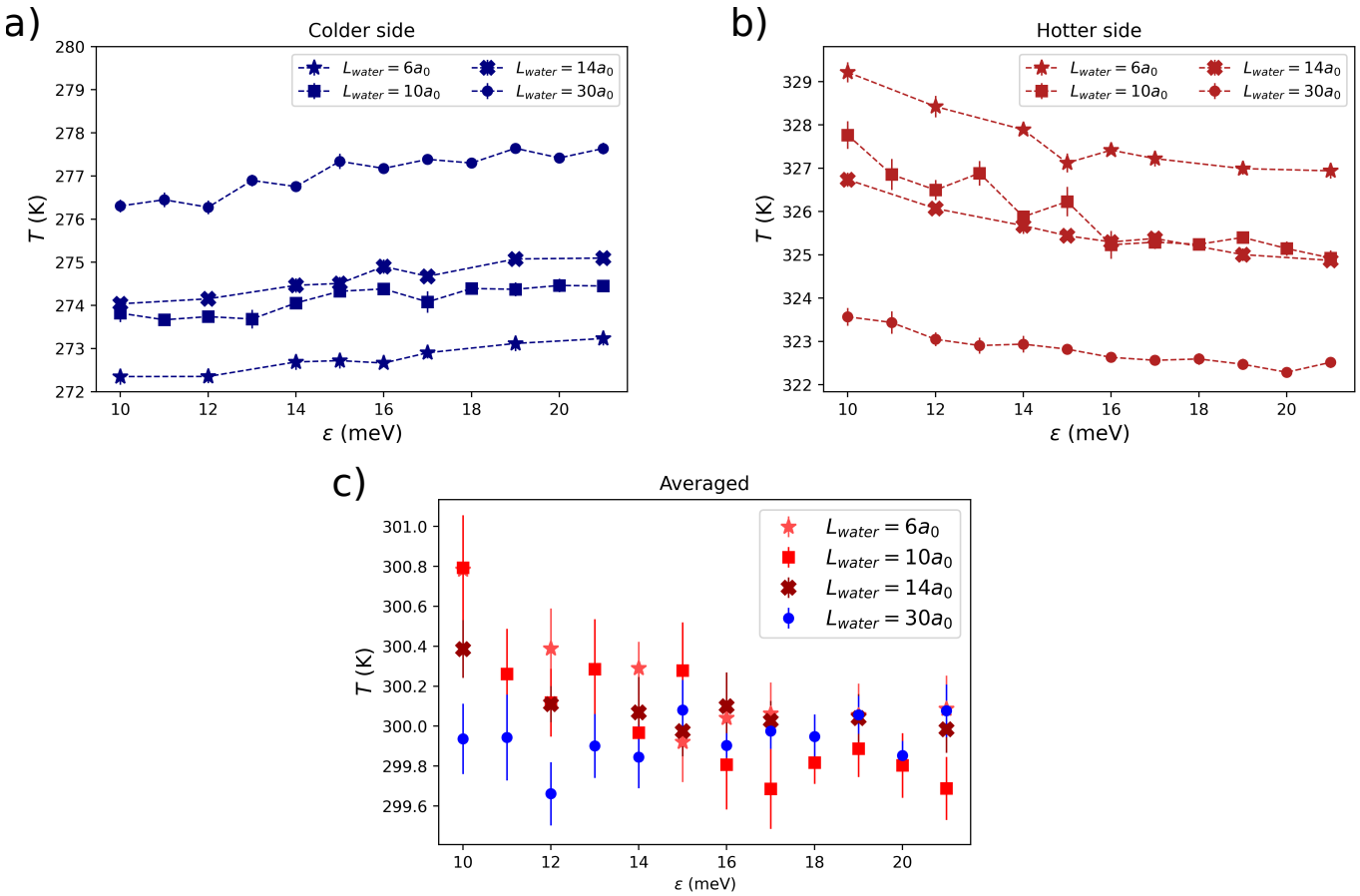

Fig. 4 Surface temperature as a function of ε for the (a) colder, (b) hotter sides and (c) averaged values.

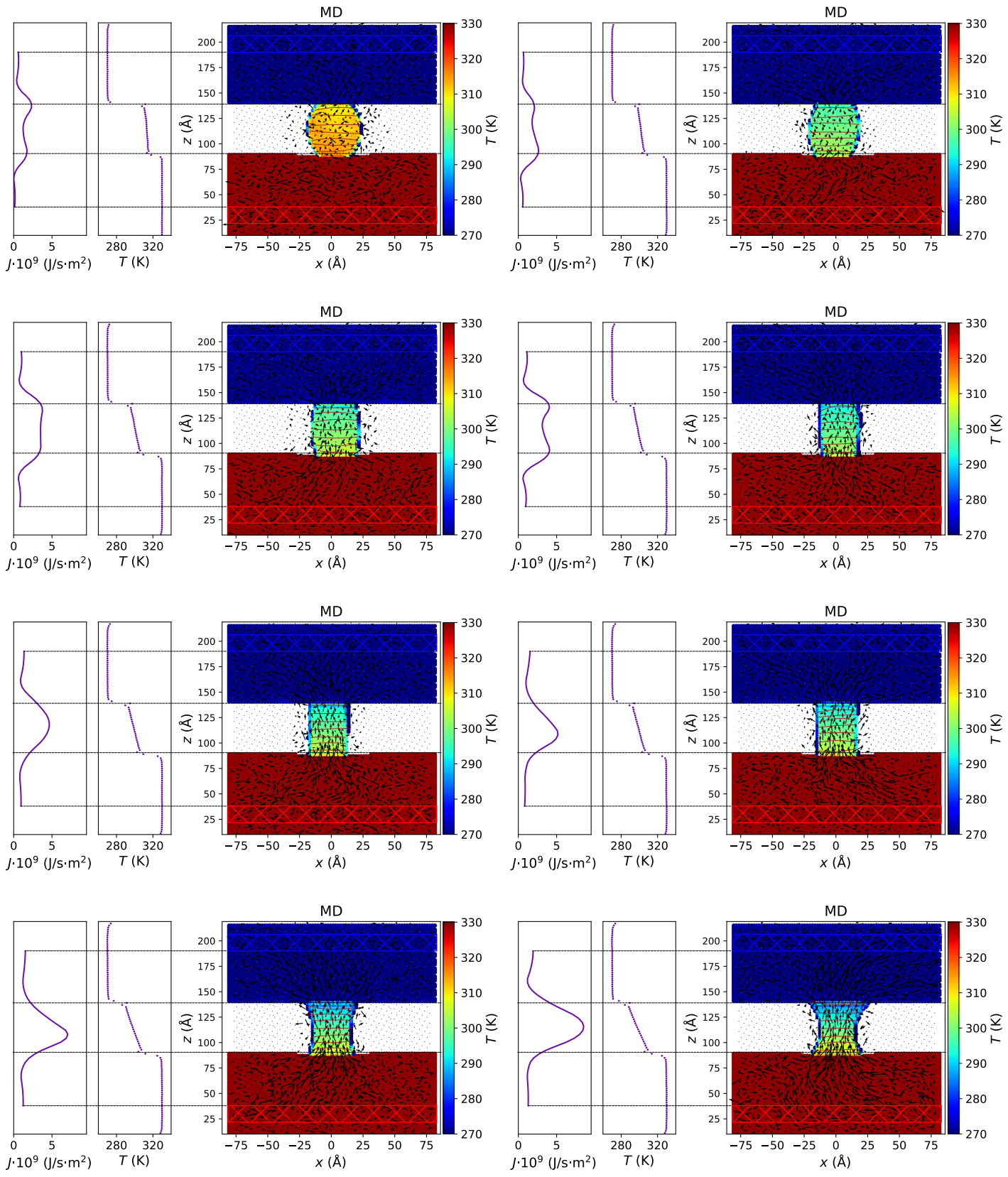

Fig. 5 Temperature profiles of the meniscus with size $6a_0$, (ε = 10 - 21 meV) with heat fluxes distributions obtained from MD simulations.

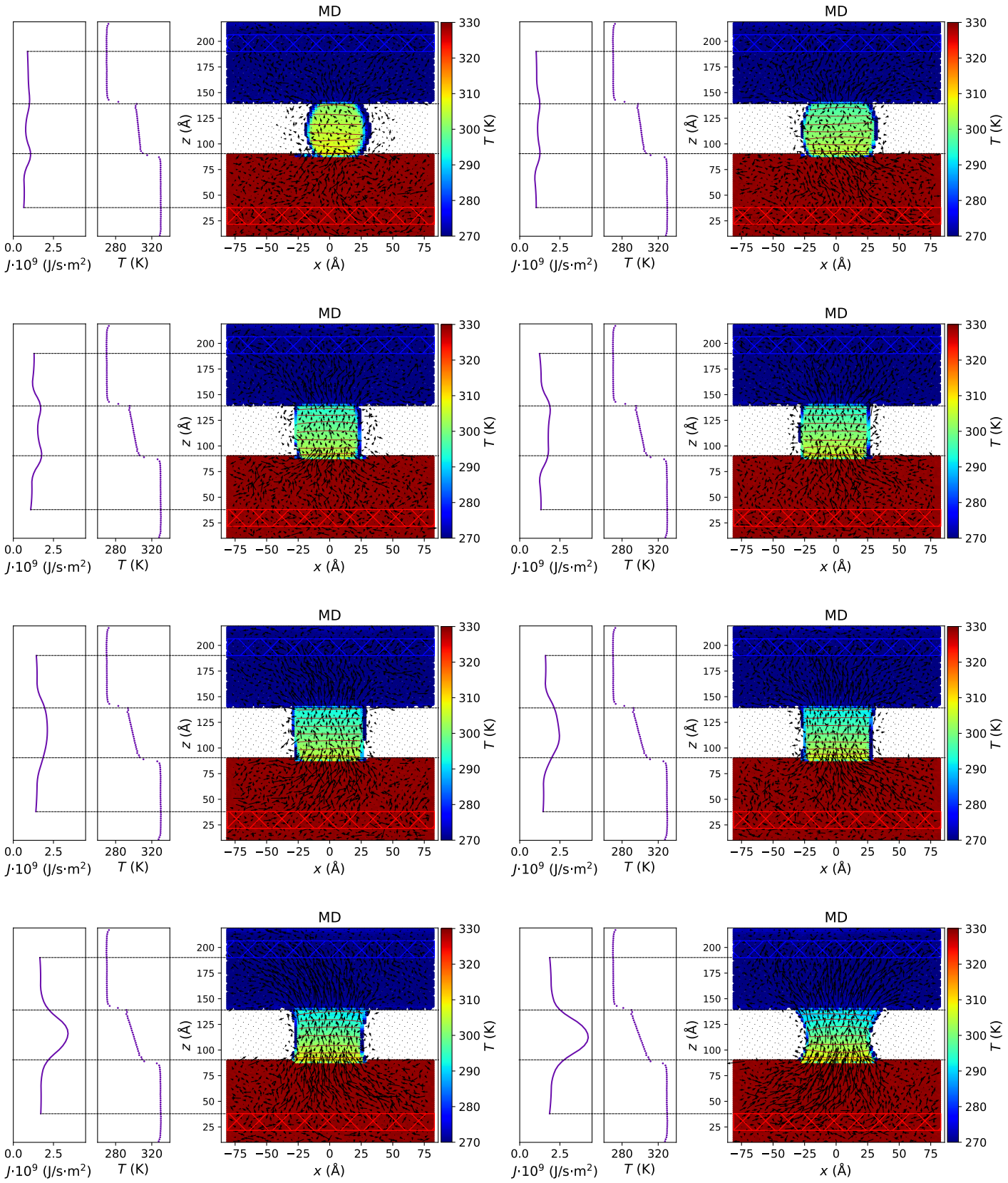

Fig. 6 Temperature profiles of the meniscus with size $10a_0$, (ε = 10 - 21 meV) with heat fluxes distributions obtained from MD simulations.

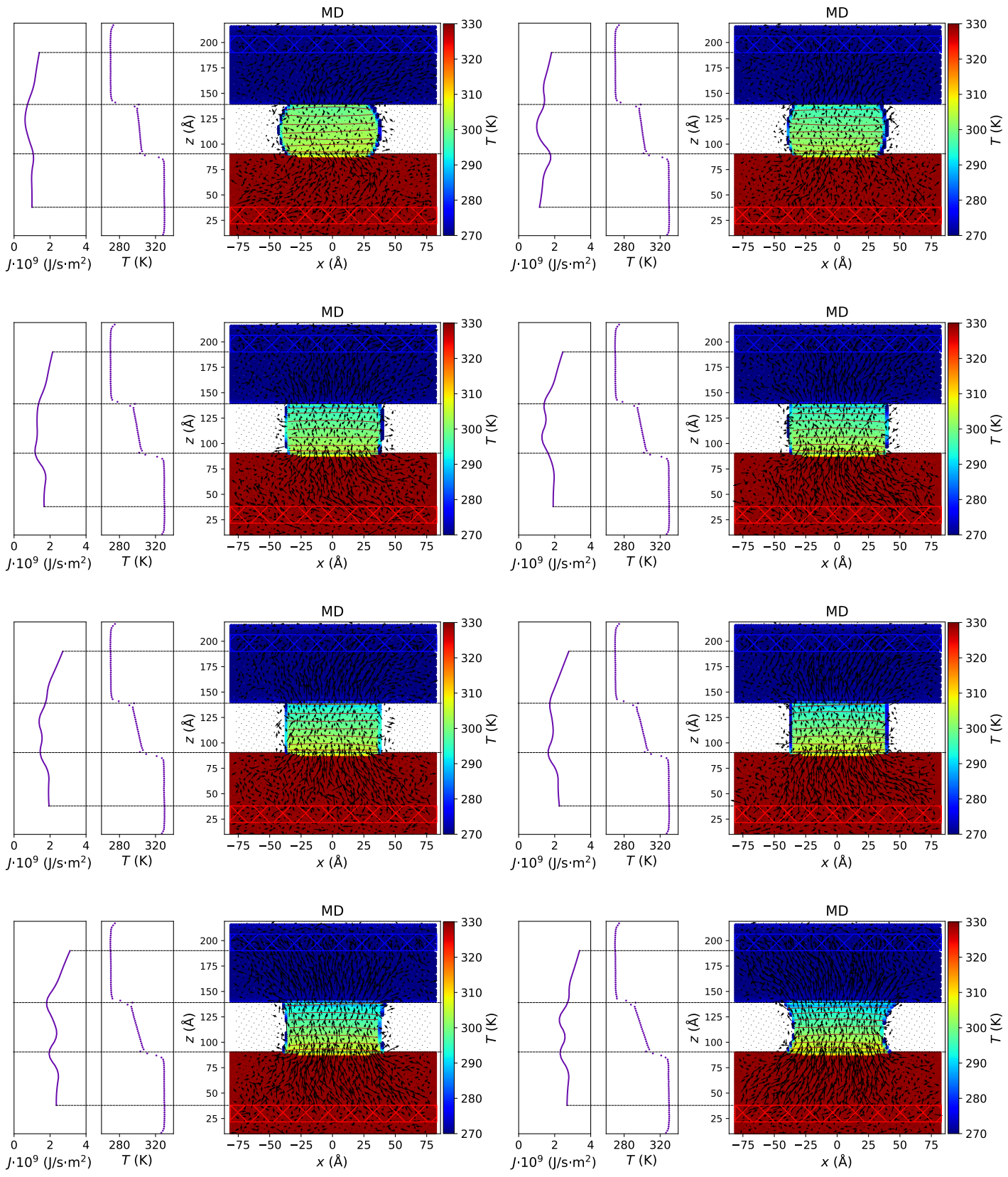

Fig. 7 Temperature profiles of the meniscus with size $14a_0$, (ε = 10 - 21 meV) with heat fluxes distributions obtained from MD simulations.

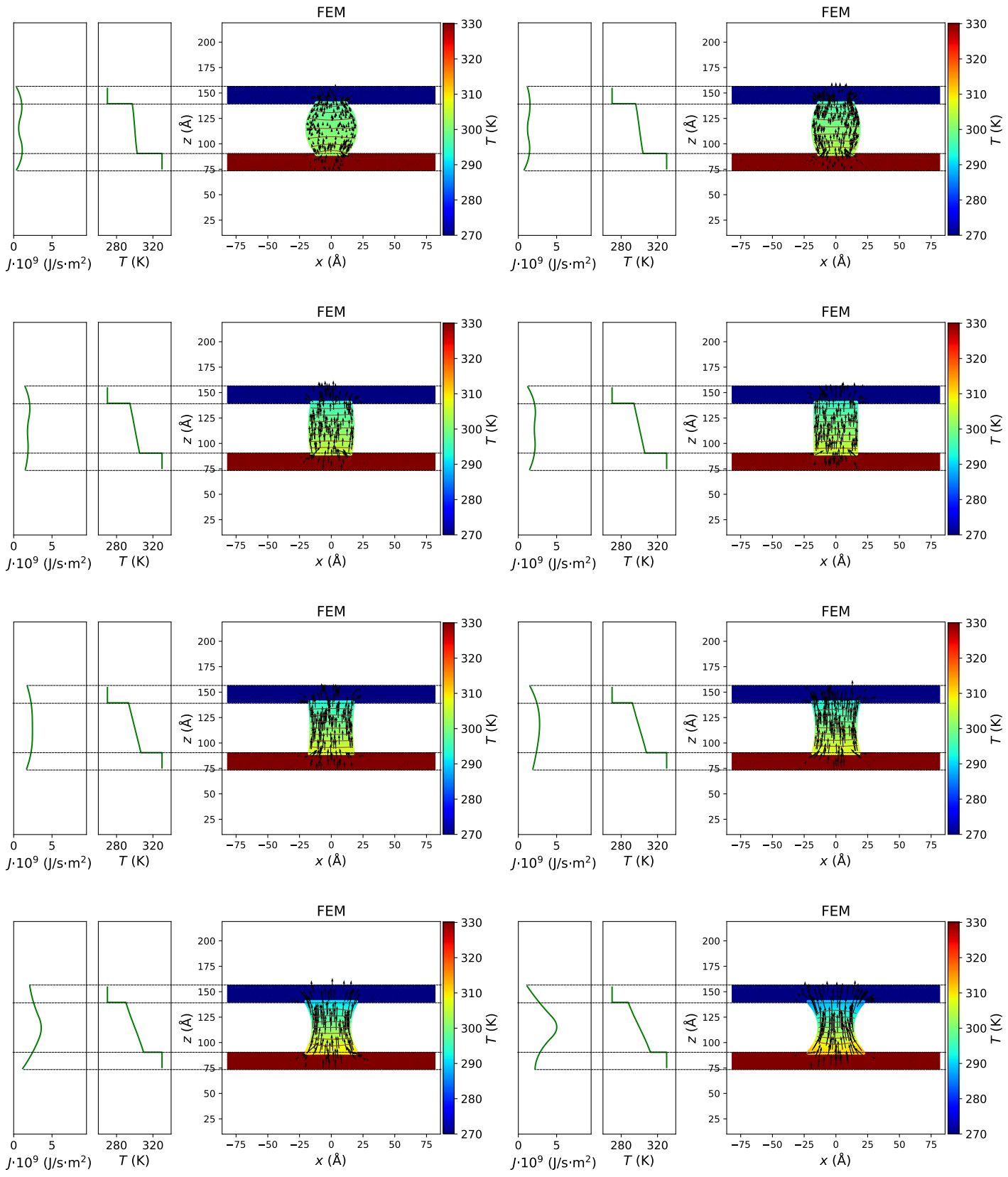

Fig. 8 Temperature profiles of the meniscus with size $6a_0$, (ε = 10 - 21 meV) with heat fluxes distributions obtained from FEM simulations.

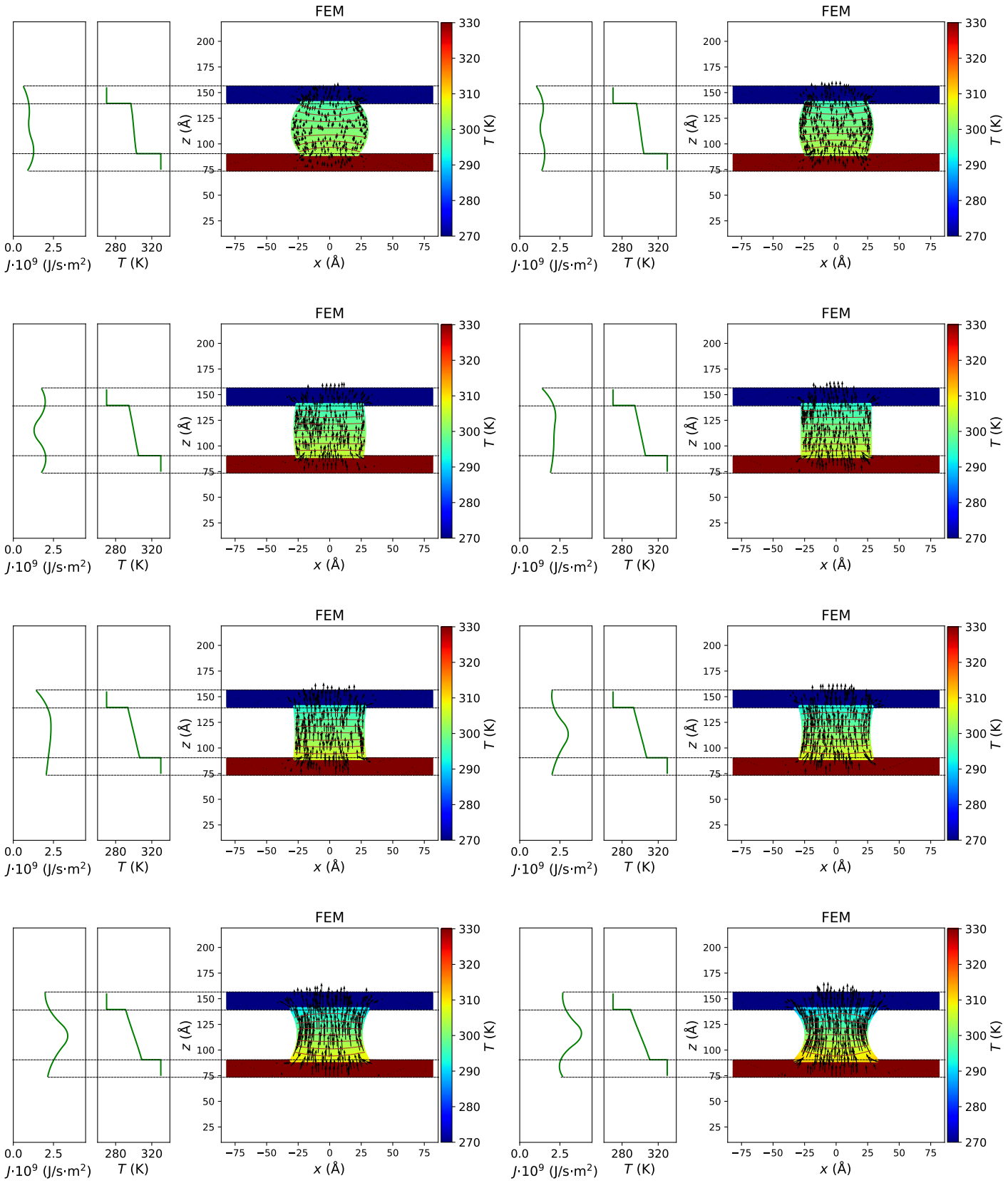

Fig. 9 Temperature profiles of the meniscus with size $10a_0$, (ε = 10 - 21 meV) with heat fluxes distributions obtained from FEM simulations.

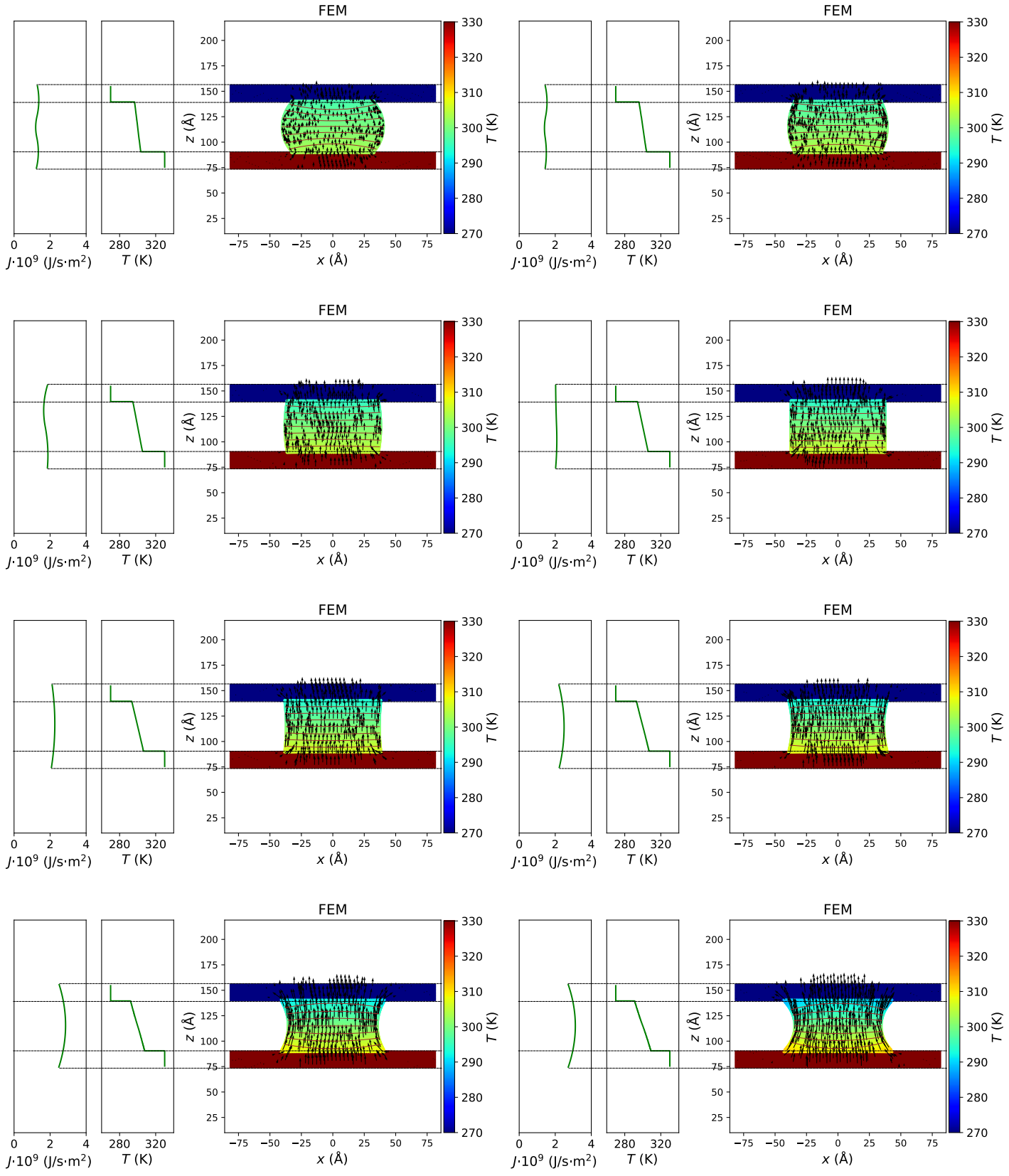

Fig. 10 Temperature profiles of the meniscus with size $14a_0$, (ε = 10 - 21 meV) with heat fluxes distributions obtained from FEM simulations.

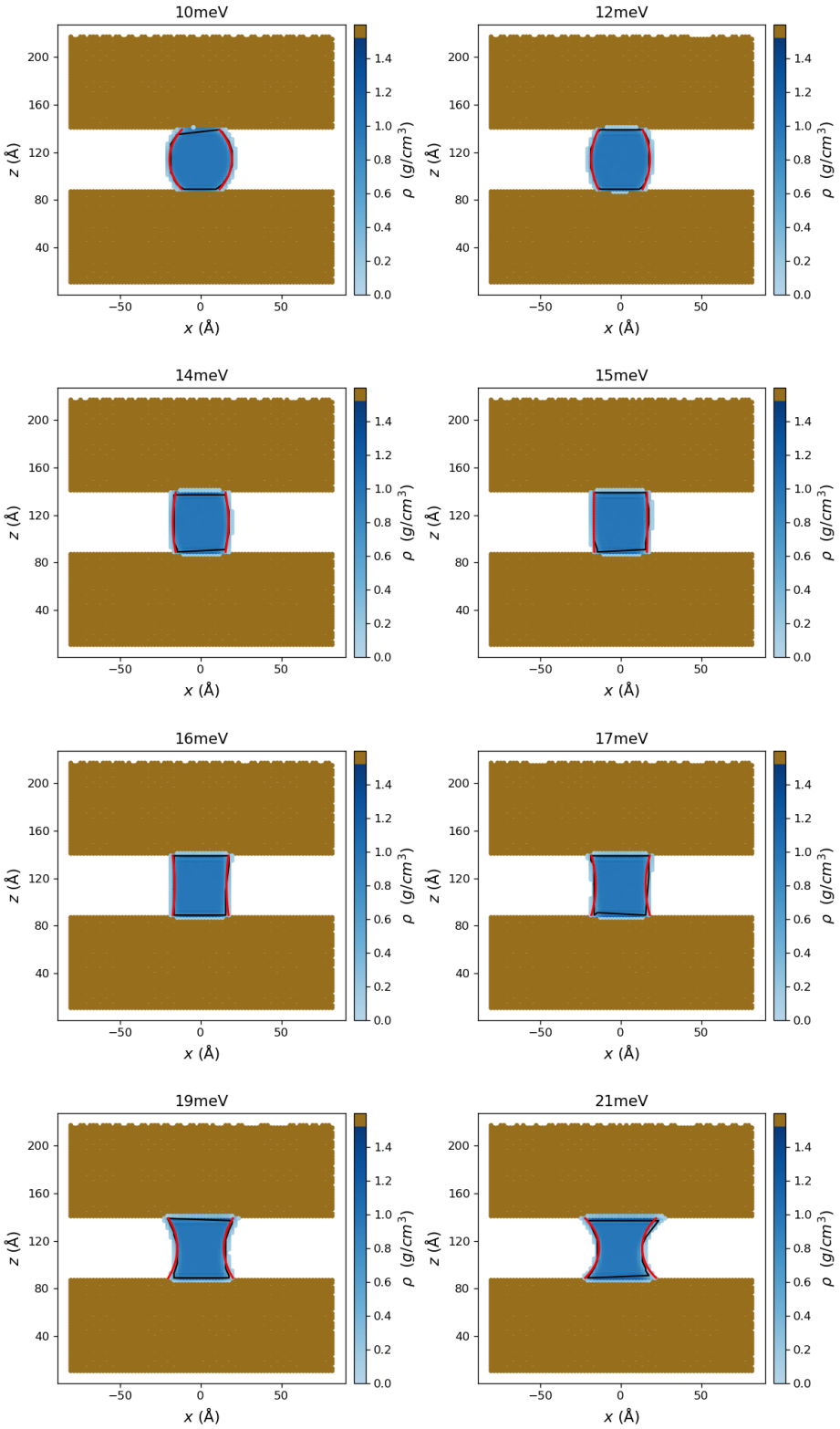

Fig. 11 The density profiles of meniscus with size $6a_0$ for different parametrization, (ε = 10 - 21 meV). Values of density are shown in colorbar. The black solid line connects the points where the density of meniscus is equal to the half of the density of confined water. Red lines are the analytically obtained borders of droplet.

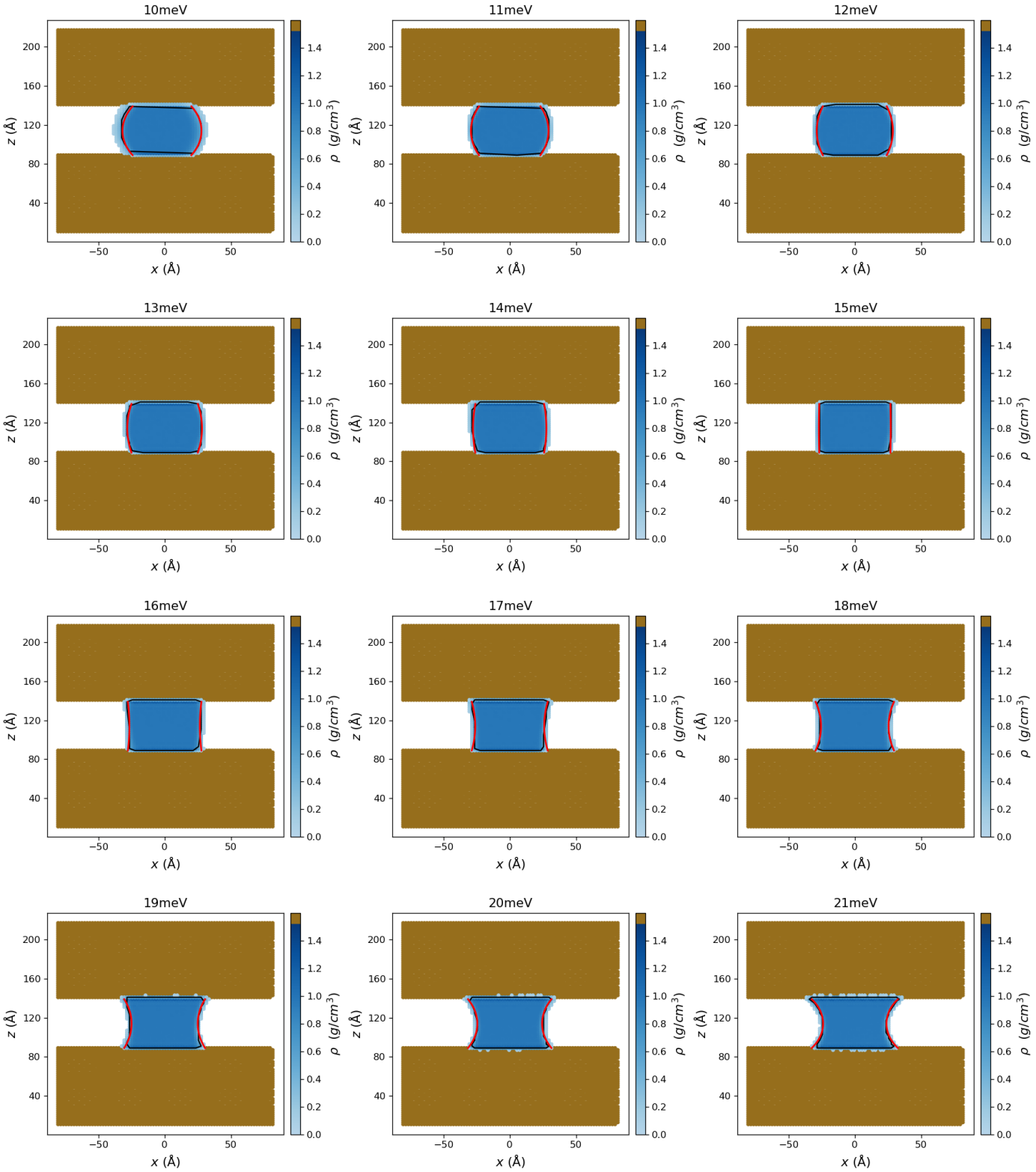

Fig. 12 The density profiles of meniscus with size $10a_0$ for different parametrization, (ε = 10 - 21 meV). Values of density are shown in colorbar. The black solid line connects the points where the density of meniscus is equal to the half of the density of confined water. Red lines are the analytically obtained borders of droplet.

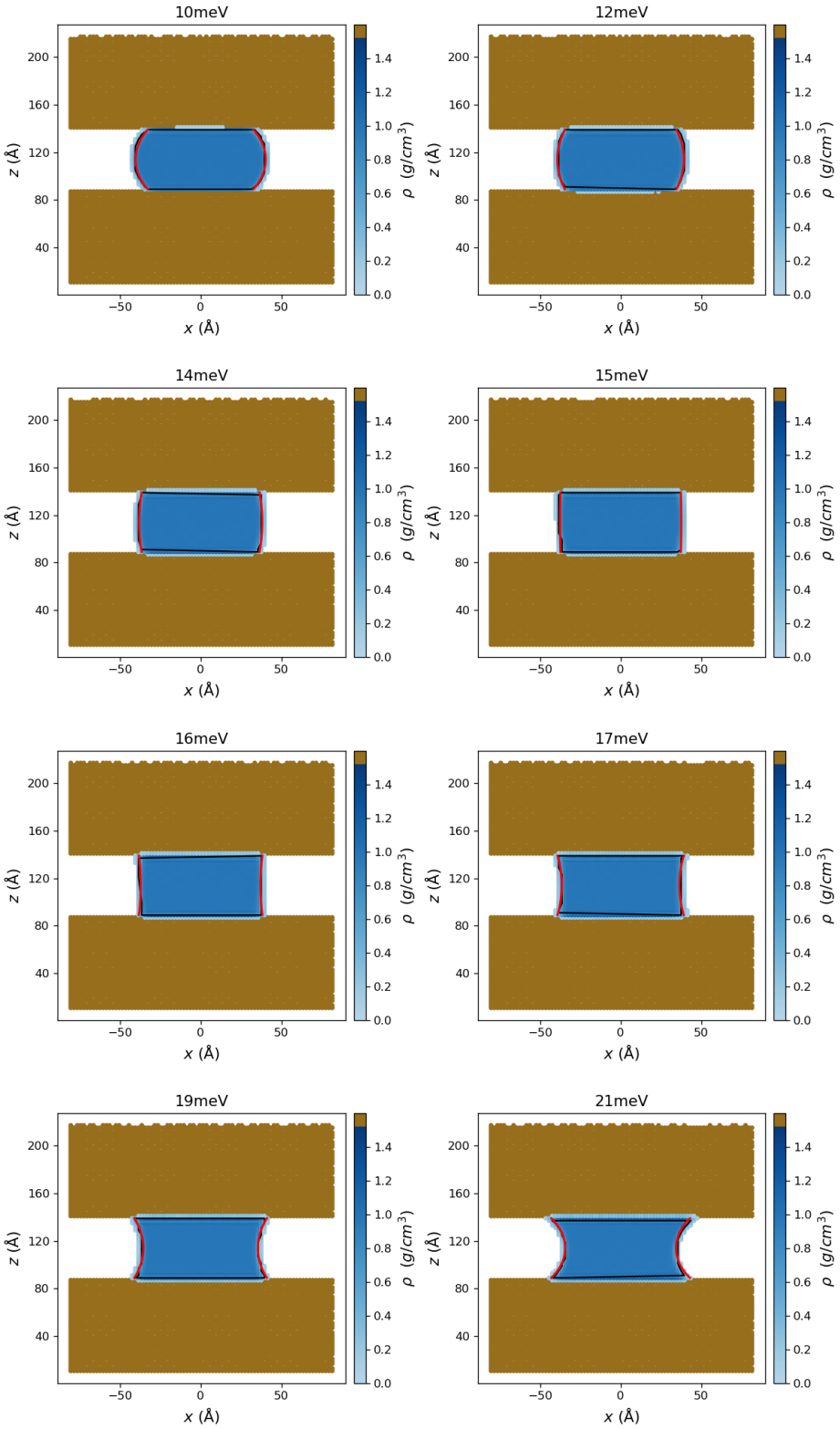

Fig. 13 The density profiles of meniscus with size $14a_0$ for different parametrization, (ε = 10 - 21 meV). Values of density are shown in colorbar. The black solid line connects the points where the density of meniscus is equal to the half of the density of confined water. Red lines are the analytically obtained borders of droplet.

Notes and references

1 F. H. Stillinger, T. A. Weber, Computer simulation of local order in condensed phases of silicon, Physical Review B 31 (8) (1985) 5262–5271. doi:10.1103/physrevb.31.5262.
URL https://doi.org/10.1103/physrevb.31.5262

2 M. Orsi, Comparative assessment of the ELBA coarse-grained model for water, Molecular Physics 112 (11) (2013) 1566–1576. doi:10.1080/00268976.2013.844373.
URL https://doi.org/10.1080/00268976.2013.844373

3 D. Andrusenko, M. Isaiev, A. Tytarenko, V. Lysenko, R. Burbelo, Size evaluation of the fine morphological features of porous nanostructures from the perturbation of heat transfer by a pore filling agent, Microporous and Mesoporous Materials 194 (2014) 79–82. doi:https://doi.org/10.1016/j.micromeso.2014.03.045.
URL https://www.sciencedirect.com/science/article/pii/S1387181114001784

4 P. Lishchuk, D. Andrusenko, M. Isaiev, V. Lysenko, R. Burbelo, Investigation of thermal transport properties of porous silicon by photoacoustic technique, International Journal of Thermophysics 36 (9) (2015) 2428–2433. doi:10.1007/s10765-015-1849-8.
URL https://doi.org/10.1007/s10765-015-1849-8

5 N. Ali, J. A. Teixeira, A. Addali, A review on nanofluids: Fabrication, stability, and thermophysical properties, Journal of Nanomaterials 2018 (2018) 1–33. doi:10.1155/2018/6978130.
URL https://doi.org/10.1155/2018/6978130

6 S. Merabia, S. Shenogin, L. Joly, P. Keblinski, J.-L. Barrat, Heat transfer from nanoparticles: A corresponding state analysis, Proceedings of the National Academy of Sciences 106 (36) (2009) 15113–15118. doi:10.1073/pnas.0901372106.
URL https://doi.org/10.1073/pnas.0901372106

7 M. Frank, D. Drikakis, Thermodynamics at solid–liquid interfaces, Entropy 20 (5) (2018) 362. doi:10.3390/e20050362.
URL https://doi.org/10.3390/e20050362

8 H. Acharya, N. J. Mozdzierz, P. Keblinski, S. Garde, How chemistry, nanoscale roughness, and the direction of heat flow affect thermal conductance of solid–water interfaces, Industrial & Engineering Chemistry Research 51 (4) (2011) 1767–1773. doi:10.1021/ie2010274.
URL https://doi.org/10.1021/ie2010274

9 N. Shenogina, R. Godawat, P. Keblinski, S. Garde, How wetting and adhesion affect thermal conductance of a range of hydrophobic to hydrophilic aqueous interfaces, Physical Review Letters 102 (15) (Apr. 2009). doi:10.1103/physrevlett.102.156101.
URL https://doi.org/10.1103/physrevlett.102.156101

10 S. Alosious, S. K. Kannam, S. P. Sathian, B. D. Todd, Prediction of kapitza resistance at fluid-solid interfaces, The Journal of Chemical Physics 151 (19) (2019) 194502. doi:10.1063/1.5126887.
URL https://doi.org/10.1063/1.5126887

11 B. Ramos-Alvarado, S. Kumar, Spectral analysis of the heat flow across crystalline and amorphous si–water interfaces, The Journal of Physical Chemistry C 121 (21) (2017) 11380–11389. doi:10.1021/acs.jpcc.7b01689.
URL https://doi.org/10.1021/acs.jpcc.7b01689

12 C. U. Gonzalez-Valle, B. Ramos-Alvarado, Spectral mapping of thermal transport across SiC-water interfaces, International Journal of Heat and Mass Transfer 131 (2019) 645–653. doi:10.1016/j.ijheatmasstransfer.2018.11.101.
URL https://doi.org/10.1016/j.ijheatmasstransfer.2018.11.101

13 C. U. Gonzalez-Valle, L. E. Paniagua-Guerra, B. Ramos-Alvarado, Implications of the interface modeling approach on the heat transfer across graphite–water interfaces, The Journal of Physical Chemistry C 123 (36) (2019) 22311–22323. doi:10.1021/acs.jpcc.9b05680.
URL https://doi.org/10.1021/acs.jpcc.9b05680

14 Y. Zhang, D. Ma, Y. Zang, X. Wang, N. Yang, A modified theoretical model to accurately account for interfacial roughness in predicting the interfacial thermal conductance, Frontiers in Energy Research 6 (2018). doi:10.3389/fenrg.2018.00048.
URL https://doi.org/10.3389/fenrg.2018.00048

15 S. Plimpton, Fast parallel algorithms for short-range molecular dynamics, Journal of Computational Physics 117 (1) (1995) 1–19. doi:https://doi.org/10.1006/jcph.1995.

1039.
URL https://www.sciencedirect.com/science/article/pii/S002199918571039X

16 Large-scale atomic/molecular massively parallel simulator, https://www.lammps.org.

17 M. Isaiev, S. Burian, L. Bulavin, M. Gradeck, F. Lemoine, K. Termentzidis, Efficient tuning of potential parameters for liquid–solid interactions, Molecular Simulation 42 (11) (2016) 910–915. doi:10.1080/08927022.2015.1105372.
URL https://doi.org/10.1080/08927022.2015.1105372

18 T. Ikeshoji, B. Hafskjold, Non-equilibrium molecular dynamics calculation of heat conduction in liquid and through liquid-gas interface, Molecular Physics 81 (2) (1994) 251–261. doi:10.1080/00268979400100171.
URL https://doi.org/10.1080/00268979400100171

19 D. Surblys, H. Matsubara, G. Kikugawa, T. Ohara, Application of atomic stress to compute heat flux via molecular dynamics for systems with many-body interactions, Physical Review E 99 (5) (May 2019). doi:10.1103/physreve.99.051301.
URL https://doi.org/10.1103/physreve.99.051301

20 P. Boone, H. Babaei, C. E. Wilmer, Heat flux for many-body interactions: Corrections to LAMMPS, Journal of Chemical Theory and Computation 15 (10) (2019) 5579–5587. doi:10.1021/acs.jctc.9b00252.
URL https://doi.org/10.1021/acs.jctc.9b00252

21 P. L. Kapitza, Heat transfer and superfluidity of helium ii, Phys. Rev. 60 (1941) 354–355. doi:10.1103/PhysRev.60.354.
URL https://link.aps.org/doi/10.1103/PhysRev.60.354

22 R. J. Stoner, H. J. Maris, Kapitza conductance and heat flow between solids at temperatures from 50 to 300 k, Physical Review B 48 (22) (1993) 16373–16387. doi:10.1103/physrevb.48.16373.
URL https://doi.org/10.1103/physrevb.48.16373

23 R. J. Stevens, A. N. Smith, P. M. Norris, Measurement of thermal boundary conductance of a series of metal-dielectric interfaces by the transient thermoreflectance technique, Journal of Heat Transfer 127 (3) (2005) 315–322. doi:10.1115/1.1857944.
URL https://doi.org/10.1115/1.1857944

24 M. Isaiev, X. Wang, K. Termentzidis, D. Lacroix, Thermal transport enhancement of hybrid nanocomposites, impact of confined water inside nanoporous silicon, Applied Physics Letters 117 (3) (2020) 033701. doi:10.1063/5.0014680.
URL https://doi.org/10.1063/5.0014680

25 C. Kunkelmann, K. Ibrahem, N. Schweizer, S. Herbert, P. Stephan, T. Gambaryan-Roisman, The effect of three-phase contact line speed on local evaporative heat transfer: Experimental and numerical investigations, International Journal of Heat and Mass Transfer 55 (7) (2012) 1896–1904. doi:https://doi.org/10.1016/j.ijheatmasstransfer.2011.11.044.
URL https://www.sciencedirect.com/science/article/pii/S0017931011006818

26 P. A. Raghupathi, On contact line region heat transfer, bubble dynamics and substrate effectsduringboiling, Ph.D. thesis, Kate Gleason College of Engineering, Rochester Institute of Technology,Rochester, New York (2018).

27 M. Barisik, A. Beskok, Temperature dependence of thermal resistance at the water/silicon interface, International Journal of Thermal Sciences 77 (2014) 47–54. doi:10.1016/j.ijthermalsci.2013.10.012.
URL https://doi.org/10.1016/j.ijthermalsci.2013.10.012

28 O. Mahian, E. Bellos, C. N. Markides, R. A. Taylor, A. Alagumalai, L. Yang, C. Qin, B. J. Lee, G. Ahmadi, M. R. Safaei, S. Wongwises, Recent advances in using nanofluids in renewable energy systems and the environmental implications of their uptake, Nano Energy 86 (2021) 106069. doi:https://doi.org/10.1016/j.nanoen.2021.106069.
URL https://www.sciencedirect.com/science/article/pii/S2211285521003268

29 H. M. R. Gonçalves, R. F. P. Pereira, E. Lepleux, L. Pacheco, A. J. M. Valente, A. J. Duarte, V. de Zea Bermudez, Non-newtonian thermosensitive nanofluid based on carbon dots functionalized with ionic liquids, Small 16 (28) (2020) 1907661. arXiv:https://onlinelibrary.wiley.com/doi/pdf/10.1002/smll.201907661, doi:https://doi.org/10.1002/smll.201907661.
URL https://onlinelibrary.wiley.com/doi/abs/10.1002/smll.201907661

30 C. U. Gonzalez-Valle, B. Ramos-Alvarado, Molecular dynamics simulations of wettability, thermal transport, and interfacial liquid structuring at the nanoscale in polar solid–liquid interfaces, ACS Applied Nano Materials 4 (4) (2021) 3821–3832. arXiv:https://doi.org/10.1021/acsanm.1c00247, doi:10.1021/acsanm.1c00247.
URL https://doi.org/10.1021/acsanm.1c00247

31 T. Kim, S. Kim, E. Kim, T. Kim, J. Cho, C. Song, S. Baik, High-Temperature Skin Softening Materials Overcoming the Trade-Off between Thermal Conductivity and Thermal Contact Resistance, Small 17 (38) (2021) 2102128. doi:10.1002/smll.202102128.
URL https://onlinelibrary.wiley.com/doi/10.1002/smll.202102128

32 D. M. Basavaraja, R. Kumar, A. K. Das, Electric Charge-Induced Active Control of Nucleate and Rapid Film Boiling at the Nanoscale: A Molecular Perspective, Langmuir 37 (33) (2021) 10006–10019. doi:10.1021/acs.langmuir.1c01144.

33 A. Azimi Yancheshme, G. Momen, R. Jafari Aminabadi, Mechanisms of ice formation and propagation on superhydrophobic surfaces: A review, Advances in Colloid and Interface Science 279 (2020) 102155. doi:10.1016/j.cis.2020.102155.
URL https://doi.org/10.1016/j.cis.2020.102155

34 J. Qiu, D. Huo, Y. Xia, Phase-Change Materials for Controlled Release and Related Applications, Advanced Materials 32 (25) (2020) 1–21. doi:10.1002/adma.202000660.

35 R. Jilte, A. Afzal, S. Panchal, A novel battery thermal management system using nano-enhanced phase change materials, Energy 219 (2021) 119564. doi:10.1016/j.energy.2020.119564.
URL https://doi.org/10.1016/j.energy.2020.119564

36 X. Yan, J. Xu, Z. Meng, J. Xie, H. Wang, A New Mechanism of Light-Induced Bubble Growth to Propel Microbubble Piston Engine, Small 16 (29) (2020) 1–15. doi:10.1002/smll.202001548.

37 D. Li, Y. Yang, D. Li, J. Pan, C. Chu, G. Liu, Organic Sonosensitizers for Sonodynamic Therapy: From Small Molecules and Nanoparticles toward Clinical Development, Small 2101976 (2021) 1–20. doi:10.1002/smll.202101976.

38 L. D. Landau, E. M. Lifshitz, Fluid Mechanics, Second Edition: Volume 6 (Course of Theoretical Physics), 2nd Edition, Course of theoretical physics / by L. D. Landau and E. M. Lifshitz, Vol. 6, Butterworth-Heinemann, 1987.

39 H. G. Ozcelik, A. C. Ozdemir, B. Kim, M. Barisik, Wetting of single crystalline and amorphous silicon surfaces: effective range of intermolecular forces for wetting, Molecular Simulation 46 (3) (2020) 224–234. arXiv:https://doi.org/10.1080/08927022.2019.1690145, doi:10.1080/08927022.2019.1690145.
URL https://doi.org/10.1080/08927022.2019.1690145

40 O. Yenigun, M. Barisik, Effect of nano-film thickness on thermal resistance at water/silicon interface, International Journal of Heat and Mass Transfer 134 (2019) 634–640. doi:https://doi.org/10.1016/j.ijheatmasstransfer.2019.01.075.
URL https://www.sciencedirect.com/science/article/pii/S0017931018353778

41 O. Yenigun, M. Barisik, Local heat transfer control using liquid dielectrophoresis at graphene/water interfaces, International Journal of Heat and Mass Transfer 166 (2021) 120801. doi:https://doi.org/10.1016/j.ijheatmasstransfer.2020.120801.
URL https://www.sciencedirect.com/science/article/pii/S001793102033739X

42 N. Wu, L. Zeng, T. Fu, Z. Wang, C. Lu, Molecular dynamics study of rapid boiling of thin liquid water film on smooth copper surface under different wettability conditions, International Journal of Heat and Mass Transfer 147 (2020) 118905. doi:https://doi.org/10.1016/j.ijheatmasstransfer.2019.118905.
URL https://www.sciencedirect.com/science/article/pii/S0017931019324251

43 N. Wu, L. Zeng, T. Fu, Z. Wang, X. Deng, Mechanism of heat transfer enhancement by nanochannels copper plate interface wettability: A molecular dynamics study, International Journal of Thermal Sciences 159 (2021) 106589. doi:https://doi.org/10.1016/j.ijthermalsci.2020.106589.
URL https://www.sciencedirect.com/science/article/pii/S1290072920310401

44 S. Aktershev, E. Chinnov, E. Shatskiy, Thermocapillary rivulets in a locally heated falling liquid film, International Journal of Heat and Mass Transfer 143 (2019) 118503. doi:https://doi.org/10.1016/j.ijheatmasstransfer.2019.118503.
URL https://www.sciencedirect.com/science/article/pii/S0017931019314449

45 E. Chinnov, E. Shatskiy, V. Semionov, Effect of thermocapillary instability on liquid film breakdown, International Journal of Heat and Mass Transfer 145 (2019) 118692. doi:https://doi.org/10.1016/j.ijheatmasstransfer.2019.118692.
URL https://www.sciencedirect.com/science/article/pii/S0017931018326954

46 G. Kuznetsov, K. Ponomarev, D. Feoktistov, E. Orlova, H. Ouerdane, Y. Lyulin, New approach to the heat transfer modeling in the coolant layer on the lower cover of a thermosyphon, International Journal of Heat and Mass Transfer 163 (2020) 120555. doi:https://doi.org/10.1016/j.ijheatmasstransfer.2020.120555.
URL https://www.sciencedirect.com/science/article/pii/S0017931020334918

47 S. A. Evlashin, J. V. Bondareva, T. F. Aslyamov, Y. V. Lyulin, K. I. Maslakov, K. V. Mironovich, M. A. Tarkhov, H. Ouerdane, Plasma modification of carbon nanowalls induces transition from superhydrophobic to superhydrophilic, Nanotechnology 32 (43) (2021) 435706. doi:10.1088/1361-6528/ac153f.
URL https://doi.org/10.1088/1361-6528/ac153f

48 O. Yenigun, M. Barisik, Effect of nano-film thickness on thermal resistance at water/silicon interface, International Journal of Heat and Mass Transfer 134 (2019) 634–640. doi:10.1016/j.ijheatmasstransfer.2019.01.075.
URL https://doi.org/10.1016/j.ijheatmasstransfer.2019.01.075

49 A. Singh, R. Lenin, N. K. Bari, C. Bakli, C. Bera, Mechanistic insights into surface contribution towards heat transfer in a nanofluid, Nanoscale Adv. 2 (2020) 3507–3513. doi:10.1039/D0NA00452A.

50 X. Cui, J. Wang, G. Xia, Enhanced thermal conductivity of nanofluids by introducing janus particles, Nanoscale 14 (2022) 99–107. doi:10.1039/D1NR05630A.
URL http://dx.doi.org/10.1039/D1NR05630A

51 X. Hou, M. Wang, L. Fu, Y. Chen, N. Jiang, C.-T. Lin, Z. Wang, J. Yu, Boron nitride nanosheet nanofluids for enhanced thermal conductivity, Nanoscale 10 (2018) 13004–13010. doi:10.1039/C8NR00651B.
URL http://dx.doi.org/10.1039/C8NR00651B

52 H. Zhan, Y. Zhou, G. Zhang, J. Zhu, W. Zhang, C. Lü, Y. Gu, Carbon nanothreads enable remarkable enhancement in the thermal conductivity of polyethylene, Nanoscale 13 (2021) 6934–6943. doi:10.1039/D1NR00356A.
URL http://dx.doi.org/10.1039/D1NR00356A

53 Y. Hong, L. Li, X. C. Zeng, J. Zhang, Tuning thermal contact conductance at graphene–copper interface via surface nanoengineering, Nanoscale 7 (2015) 6286–6294. doi:10.1039/C5NR00564G.
URL http://dx.doi.org/10.1039/C5NR00564G

54 E. T. Swartz, R. O. Pohl, Thermal boundary resistance, Rev. Mod. Phys. 61 (1989) 605–668. doi:

10.1103/RevModPhys.61.605.
URL https://link.aps.org/doi/10.1103/RevModPhys.61.605

55 A. Assy, S. Lefèvre, P.-O. Chapuis, S. Gomès, Analysis of heat transfer in the water meniscus at the tip-sample contact in scanning thermal microscopy, Journal of Physics D: Applied Physics 47 (2014) 442001. doi:10.1088/0022-3727/47/44/442001.

56 J. Bodzenta, A. Kaźmierczak-Bałata, K. Harris, Quantitative thermal measurement by the use of scanning thermal microscope and resistive thermal probes, Journal of Applied Physics 127 (3) (2020) 031103. doi:10.1063/1.5125062.

57 Y. Zhang, W. Zhu, F. Hui, M. Lanza, T. Borca-Tasciuc, M. Muñoz Rojo, A review on principles and applications of scanning thermal microscopy (sthm), Advanced Functional Materials 30 (18) (2020) 1900892. doi:https://doi.org/10.1002/adfm.201900892.